Vietnam Journal of Mechanics, Vol. 45, No. 1 (2023), pp. 75 – 90
DOI: https://doi.org/10.15625/0866-7136/17956

BUCKLING ANALYSIS OF LAMINATED COMPOSITE THIN-WALLED I-BEAM UNDER MECHANICAL AND THERMAL LOADS

Xuan-Bach Bui[1], **Anh-Cao Nguyen**[1], **Ngoc-Duong Nguyen**[1,*], **Tien-Tho Do**[1], **Trung-Kien Nguyen**[2]
[1]*Ho Chi Minh City University of Technology and Education, 1 Vo Van Ngan Street, Thu Duc City, Ho Chi Minh City, Vietnam*
[2]*CIRTech Institute, HUTECH University, 475A Dien Bien Phu Street, Binh Thanh District, Ho Chi Minh City, Vietnam*
[*]E-mail: duongnn@hcmute.edu.vn

Received: 17 December 2022 / Published online: 20 March 2023

Abstract. Despite the extensive use of thin-walled structures, the studies on their behaviours when exposed to extreme thermal environment are relatively scarce. Therefore, this paper aims to present the buckling analysis of thin-walled composite I-beams under thermo-mechanical loads. The thermal effects are investigated for the case of studied beams undergoing a uniform temperature rise through their thickness. The theory is based on the first-order shear deformation thin-walled beam theory with linear variation of displacements in the wall thickness. The governing equations of motion are derived from Hamilton's principle and are solved by series-type solutions with hybrid shape functions. Numerical results are presented to investigate the effects of fibre angle, material distribution, span-to-height's ratio and shear deformation on the critical buckling load and temperature rise. These results for several cases are verified with available references to demonstrate the present beam model's accuracy.

Keywords: thin-walled beam, thermal buckling, buckling analysis, series solution.

1. INTRODUCTION

The application of anisotropic laminated composite materials is increasing in many engineering fields such as aerospace, aircrafts and civil [1–4]. Thanks to its excellent mechanical properties, especially the strength-to-weight ratio, such structures have become a topic of interest for many researchers, some of which, can be found in [5,6]. Comparable to the Euler-Bernoulli theory for solid beam, Vlasov [7] developed the classical thin-walled beam theory (CTWBT) which ignores the effects of shear deformation. Vlasov's theory is easy to implement and analyse LC thin-walled beams [7–10]. Nonetheless, in the case of thick short beam, Vlasov's theory deliver inaccurate beam responses predictions such as the deflection, natural frequencies and critical buckling loads. Razaqpur and Li [11] developed a finite element model for thin-walled box girder that can analyse the extension, flexure, torsion, torsional warping, distortion, distortional warping, and shear lag effects using an extended version of Vlasov's thin-walled beam theory. Pavazza et al. [12] proposed a novel torsion theory for shear deformable thin-walled beams of arbitrary open cross-sections based on the classical Vlasov's theory of thin-walled beams and the Timoshenko's beam bending theory. Comparable to the first-order shear deformation beam theory, the first-order thin-walled beam theory (FTWBT) takes the transverse shear into account and allow the transverse displacement vary linearly across the thin wall thickness. The FTWBT gives better beam responses' predictions for beam with $L/b_3 < 10$ and has been studied in multiple researches [13–23]. The FTWBT demands a shear correction factor [24] to be calculated but it can also be a source of error. To overcome this setback, the high-order deformation thin-walled beam theory (HTWBT) has been proposed [25–27]. Though the HTWBT predicts more accurate results than the FTWBT, it appears to be too complicated to implement.

Besides, in practical engineering contexts, thin-walled beams are exposed to high-temperature environments. Therefore, the predictions of the thin-walled beams' responses to the thermal load in such contexts are of utmost importance. Many models and approaches on this matter have been studied in recent years for solid beams with rectangle sections, some representative references are herein cited. Trinh et al. [28] presented an analytical method for the vibration and buckling of functionally graded beams under mechanical and thermal loads. Nguyen et al. [29] investigated the hygro-thermal effects on vibration and thermal buckling behaviours of functionally graded beams. Li et al. [30] studied the free vibration characteristics of a spinning composite thin-walled beam under hygrothermal environment. Sun et al. [31] investigated the buckling and post-buckling behaviors of functionally graded Timoshenko beams on non-linear elastic foundation. A brief literature study shows that although many researches on thermal responses of laminated composite and functionally graded beams with rectangle sections have been performed, thermal buckling behaviors of thin-walled beams are extremely limited, Simonetti et al. [32] recently presented the thermal buckling analysis of thin-walled closed section functionally graded beam-type structures [32]. Pantousa [33] conducted a numerical study on thermal buckling of empty thin-walled steel tanks under multiple pool-fire scenarios.

This paper aims to investigate the elastic buckling of laminated composite thin-walled beams with I-section in thermo-mechanical environments. It is based on the FTWBT with a uniform temperature rise. The characteristic equations are derived from Hamilton's principle and solved by Ritz method with hybrid shape functions. Numerical results are presented for the laminated composite I-beams with various boundary conditions, fibre angles and length-to-height ratios.

2. THEORETICAL FORMULATION

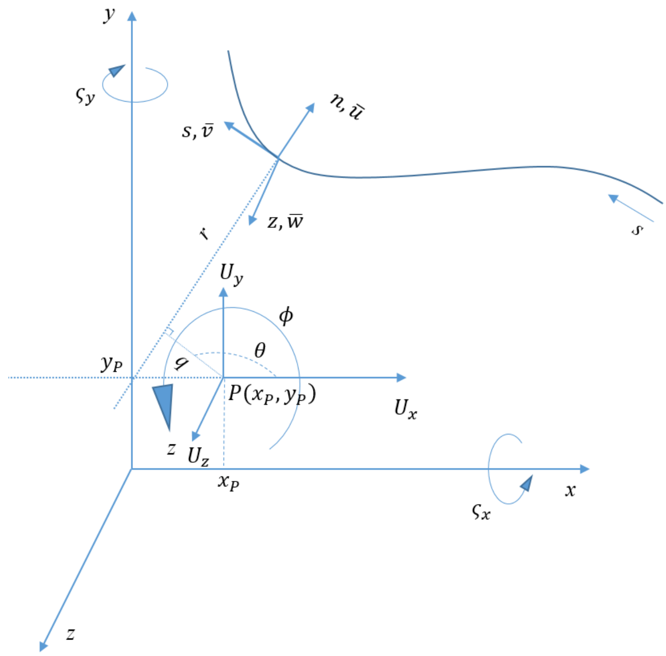

Fig. 1. Coordinate systems of a thin-walled beam

To analyse the thin-walled beam, the variables are defined in three set of coordinate systems as displayed in Fig. 1. These are the Cartesian coordinate system (x, y, z) , the local plate coordinate system (n, s, z) and the contour coordinate s along the profile of the section. The angle θ is the angle between s- and x-axes. The pole $P\,(x_P, y_P)$ is optimally chosen to be at the shear center of the section. The assumptions made in this beam model are: the effects of geometrical nonlinearity are ignored, the section contour remains undeformed in its own plane and the transverse shear strains are constant in the wall thickness. Fig. 2 shows how the aforementioned coordinate systems fit in to the thin-walled I-beam in this paper. The widths (b_1, b_2, b_3) and the thicknesses (h_1, h_2, h_3) with lower index 1, 2, 3 are for the beam's top, bottom flange, and web, respectively.

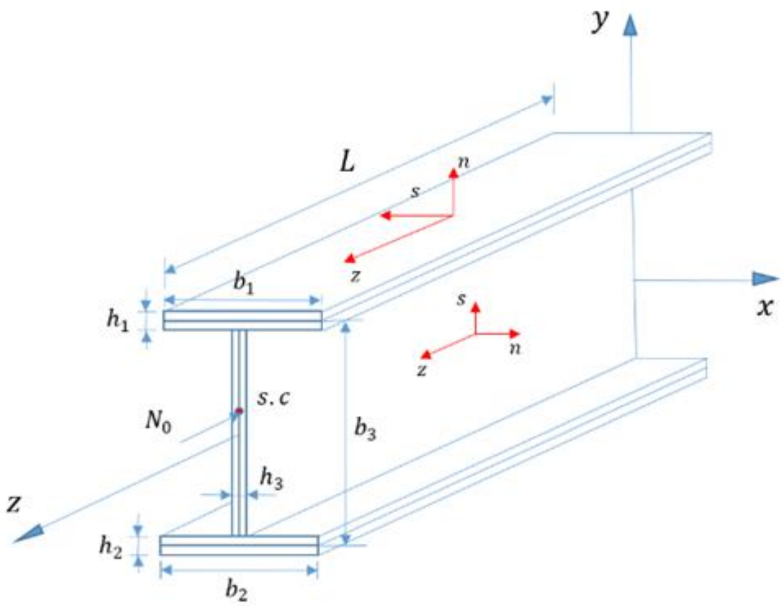

Fig. 2. Geometry of a thin-walled I-beam

2.1. Kinematics

The displacements $(\bar{u}, \bar{v}, \bar{w})$ at any point on the midsurface of the laminated composite thin-walled beams under a small rotation ϕ about the pole axis can be expressed in terms of those at the pole (U, V, W) as follows

$$\bar{u}(s,z) = U_x(z)\sin\theta(s) - U_y(z)\cos\theta(s) - \phi(z)\, q(s), \tag{1a}$$

$$\bar{v}(s,z) = U_x(z)\cos\theta(s) + U_y(z)\sin\theta(s) - \phi(z)\, r(s), \tag{1b}$$

$$\bar{w}(s,z) = U_z(z) + \varsigma_y(z)\, x(s) + \varsigma_x(z)\, y(s) + \varsigma_\omega(z)\, \omega(s), \tag{1c}$$

where $\varsigma_x, \varsigma_y, \varsigma_\omega$ are the rotations of the cross-section with respect to and, respectively, which are defined by

$$\varsigma_y = \gamma_{xz}^0 - U_x', \quad \varsigma_x = \gamma_{yz}^0 - U_y', \quad \varsigma_\omega = \gamma_\omega^0 - \phi'. \tag{2}$$

The warping function ω is given by

$$\omega(s) = \int_{s_0}^{s} r(s)\mathrm{d}s. \tag{3}$$

Moreover, the displacements (u, v, w) at a point on the beam section are expressed in term of the mid-surface displacements $(\bar{u}, \bar{v}, \bar{w})$ as follows

$$u(n,s,z) = \bar{u}(s,z), \tag{4a}$$

$$v(n,s,z) = \bar{v}(s,z) + n\bar{\varsigma}_s(s,z), \tag{4b}$$

$$w(n,s,z) = \bar{w}(s,z) + n\bar{\varsigma}_z(s,z), \tag{4c}$$

where $\bar{\varsigma}_s$ and $\bar{\varsigma}_z$ are expressed as follows

$$\bar{\varsigma}_z = \varsigma_y \sin\theta - \varsigma_x \cos\theta - \varsigma_\omega q, \quad \bar{\psi}_s(s,z,t) = -\frac{\partial u}{\partial s}. \tag{5}$$

2.2. Strains

From the displacements defined in Eq. (4), the strain field can be written as

$$\varepsilon_s(n,s,z) = \bar{\varepsilon}_s(s,z) + n\bar{\kappa}_s(s,z), \tag{6a}$$

$$\varepsilon_z(n,s,z) = \bar{\varepsilon}_z(s,z) + n\bar{\kappa}_z(s,z), \tag{6b}$$

$$\gamma_{sz}(n,s,z) = \bar{\gamma}_{sz}(s,z) + n\bar{\kappa}_{sz}(s,z), \tag{6c}$$

$$\gamma_{nz}(n,s,z) = \bar{\gamma}_{nz}(s,z) + n\bar{\kappa}_{nz}(s,z), \tag{6d}$$

where

$$\bar{\varepsilon}_s = 0, \quad \bar{\varepsilon}_z = \frac{\partial \bar{w}}{\partial z} = \varepsilon_z^0 + x\kappa_y + y\kappa_x + \omega\kappa_\omega, \quad \bar{\kappa}_s = 0, \tag{7a}$$

$$\bar{\kappa}_z = \frac{\partial \bar{\varsigma}_z}{\partial z} = \kappa_y \sin\theta - \kappa_x \cos\theta - \kappa_\omega q, \quad \bar{\kappa}_{sz} = \kappa_{sz}, \quad \bar{\kappa}_{nz} = 0, \tag{7b}$$

$$\varepsilon_z^0 = W', \quad \kappa_x = \varsigma_x', \quad \kappa_y = \varsigma_y', \quad \kappa_\omega = \varsigma_\omega', \quad \kappa_{sz} = \phi' - \varsigma_\omega, \tag{7c}$$

$$\varepsilon_z = \varepsilon_0^z + (x + n\sin\theta)\kappa_y + (y - n\cos\theta)\kappa_x + (\omega - nq)\kappa_\omega, \tag{7d}$$

$$\gamma_{sz} = \gamma_{xz}^0 \cos\theta + \gamma_{yz}^0 \sin\theta + \gamma_\omega^0 r + n\kappa_{sz}, \quad \gamma_{nz} = \gamma_{xz}^0 \sin\theta - \gamma_{yz}^0 \cos\theta - \gamma_\omega^0 q. \tag{7e}$$

2.3. Stress-strains relation

For laminated composite thin-walled beams, it is supposed to be constituted by a number of orthotropic material layers with the same thickness. The reduced constitutive equations at the k^{th}-layer is given by

$$\begin{Bmatrix} \sigma_z \\ \sigma_{sz} \\ \sigma_{nz} \end{Bmatrix} = \begin{pmatrix} P_{11} & P_{16} & 0 \\ P_{16} & P_{66} & 0 \\ 0 & 0 & P_{55} \end{pmatrix} \begin{Bmatrix} \varepsilon_z \\ \gamma_{sz} \\ \gamma_{nz} \end{Bmatrix}, \tag{8a}$$

where $P_{11} = \bar{Q}_{11} - \dfrac{\bar{Q}_{12}^2}{\bar{Q}_{22}}$, $P_{16} = \bar{Q}_{16} - \dfrac{\bar{Q}_{12}\bar{Q}_{26}}{\bar{Q}_{22}}$, $P_{66} = \bar{Q}_{66} - \dfrac{\bar{Q}_{26}^2}{\bar{Q}_{22}}$, $P_{55} = \bar{Q}_{55}$; $\bar{Q}_{ij}$ are the transformed reduced stiffness matrix elements which can be computed based on the fibre lay-up as follows

$$\bar{Q}_{11} = Q_{11}c^4 + Q_{22}s^4 + 2(Q_{12} + 2Q_{66})s^2c^2, \tag{8b}$$

$$\bar{Q}_{12} = (Q_{11} + Q_{22} - 4Q_{66})s^2c^2 + Q_{12}(s^4 + c^4), \tag{8c}$$

$$\bar{Q}_{22} = Q_{11}s^4 + 2(Q_{12} + 2Q_{66})s^2c^2 + Q_{22}c^4, \tag{8d}$$

$$\bar{Q}_{16} = (Q_{11} - Q_{12} - 2Q_{66})sc^3 + (Q_{12} - Q_{22} + 2Q_{66})s^3c, \tag{8e}$$

$$\bar{Q}_{26} = (Q_{12} - Q_{22} + 2Q_{66})sc^3 + (Q_{11} - Q_{12} - 2Q_{66})s^3c, \tag{8f}$$

$$\bar{Q}_{55} = Q_{55}c^2 + Q_{44}s^2, \tag{8g}$$

$$\bar{Q}_{66} = (Q_{11} + Q_{22} - 2Q_{12} - 2Q_{66})s^2c^2 + Q_{66}(s^4 + c^4), \tag{8h}$$

$$Q_{11} = E_1/(1-\nu_{12}\nu_{21}), \quad Q_{22} = E_2/(1-\nu_{12}\nu_{21}), \quad Q_{12} = \nu_{12}Q_{22}, \tag{8i}$$

$$Q_{44} = G_{23}, \quad Q_{55} = G_{13}, \quad Q_{66} = G_{12}, \quad s = \sin\theta, \quad c = \cos\theta, \tag{8j}$$

where θ is the fibre orientation angle of the current laminated layer, E_1 and E_2 are the Young's moduli, ν_{12} and ν_{21} are the Poisson's ratio values, G_{12}, G_{13} and G_{23} are the shear moduli of the laminated composite material.

2.4. Variational formulation

The characteristic equations of the laminated composite thin-walled beams can be derived by Hamilton's principle in which the total energy of the system Π is composed of the strain energy Π_S and work done by external force Π_W. The strain energy Π_S of the laminated composite thin-walled beam is expressed by

$$\Pi_S = \frac{1}{2}\int_\Omega \left(\sigma_z\varepsilon_z + \sigma_{sz}\gamma_{sz} + \sigma_{nz}\gamma_{nz}\right) \mathrm{d}\Omega, \tag{9}$$

where Ω is the beam volume. Substitution of Eqs. (6), (7) and (8) into Eq. (9) gives

$$\begin{aligned}
\Pi_S = \frac{1}{2}\int_0^L & [E_{11}U'^2_z + 2E_{16}U'_zU'_x + 2E_{17}U'_zU'_y + 2\left(E_{15}+E_{18}\right)U'_z\phi' \\
& + 2E_{12}U'_z\varsigma'_y + 2E_{16}U'_z\varsigma_y + 2E_{13}U'_z\varsigma'_x + 2E_{17}U'_z\varsigma_x + 2E_{14}U'_z\varsigma'_\omega \\
& + 2\left(E_{18}-E_{15}\right)U'_z\varsigma'_\omega + E_{66}U'^2_x + 2E_{67}U'_xU'_y + 2\left(E_{56}+E_{68}\right)U'_x\phi' \\
& + 2E_{26}U'_x\varsigma'_y + 2E_{66}U'_x\varsigma_y + 2E_{36}U'_x\varsigma'_x + 2E_{67}U'_x\varsigma_x + 2E_{46}U'_x\varsigma'_\omega \\
& + 2\left(E_{68}-E_{56}\right)U'_x\varsigma_\omega + E_{77}U'^2_y + 2\left(E_{57}+E_{78}\right)U'_y\phi' + 2E_{27}U'_y\varsigma'_y \\
& + 2E_{67}U'_y\varsigma'_y + 2E_{37}U'_y\varsigma'_x + 2E_{77}U'_y\varsigma_x + 2E_{47}U'_y\varsigma_\omega + 2\left(E_{78}-E_{57}\right)U'_y\varsigma_\omega \\
& + \left(E_{55}+2E_{58}+E_{88}\right)\phi'^2 + 2\left(E_{25}+E_{28}\right)\phi'\varsigma'_y + 2\left(E_{56}+E_{68}\right)\phi'\varsigma_y \\
& + 2\left(E_{78}-E_{57}\right)U'_y\varsigma_\omega + \left(E_{55}+2E_{58}+E_{88}\right)\phi'^2 + 2\left(E_{25}+E_{28}\right)\phi'\varsigma'_y \\
& + 2\left(E_{56}+E_{68}\right)\phi'\varsigma_\omega + 2\left(E_{35}+E_{38}\right)\phi'\varsigma'_x + 2\left(E_{57}+E_{78}\right)\phi'\varsigma_x \\
& + 2\left(E_{45}+E_{48}\right)\phi'\varsigma'_\omega + 2\left(E_{88}-E_{55}\right)\phi'\varsigma_\omega + E_{22}\psi'^2_y + 2E_{26}\varsigma'_y\varsigma_y \\
& + E_{66}\varsigma^2_y + 2E_{23}\varsigma'_y\varsigma'_x + 2E_{27}\varsigma'_y\varsigma_x + 2E_{36}\varsigma_y\varsigma'_x + 2E_{67}\varsigma_y\varsigma_x \\
& + E_{24}\varsigma'_y\varsigma'_\omega + 2\left(E_{28}-E_{25}\right)\varsigma'_y\varsigma_\omega + 2E_{46}\varsigma_y\varsigma_\omega + 2\left(E_{68}-E_{56}\right)\varsigma_y\varsigma_\omega \\
& + E_{33}\varsigma'^2_\omega + 2E_{37}\varsigma'_x\varsigma_x + E_{77}\varsigma^2_x + 2E_{34}\varsigma'_x\varsigma'_\omega + 2\left(E_{38}-E_{35}\right)\varsigma'_x\varsigma_\omega \\
& + 2E_{47}\varsigma_x\varsigma'_\omega + 2\left(E_{78}-E_{57}\right)\varsigma_x\varsigma_\omega + +E_{44}\varsigma'^2_\omega 2\left(E_{48}-E_{45}\right)\varsigma'_\omega\varsigma_\omega \\
& + \left(E_{88}-2E_{58}+E_{55}\right)\varsigma^2_\omega]\,\mathrm{d}z,
\end{aligned} \tag{10}$$

where E_{ij} are the stiffness coefficients of the laminated composite thin-walled composite beams [34].

The work done by the external mechanical axial load N_0^m and thermal load N_0^t is defined as

$$\Pi_W = \frac{1}{2}\int_{\Omega} \frac{\left(N_0^m + N_0^t\right)}{A} \left(u'^2 + v'^2\right) \mathrm{d}\Omega \\ = \frac{1}{2}\int_0^L \left(N_0^m + N_0^t\right) \left(U'^2_x + U'^2_y + 2y_p U'_x \phi' - 2x_p U'_y \phi' + \frac{I_p}{A}\phi'^2\right) \mathrm{d}z, \tag{11}$$

where A is the cross-sectional area; I_p is the polar moment of inertia about the centroid given by

$$I_p = I_x + I_y, \tag{12}$$

where I_x and I_y are the second moment of inertia with respect to the x- and y-axes, respectively

$$I_x = \int_A y^2 \mathrm{d}A, \quad I_y = \int_A x^2 \mathrm{d}A. \tag{13}$$

The axial thermal load is given as

$$N_0^t = \int_n \left(\alpha_z P_{11} + 2\alpha_{sz} P_{16}\right) \Delta T \mathrm{d}n, \tag{14}$$

where $\Delta T = T - T_0$ is the temperature difference; T_0 is the initial temperature; α_z, α_{sz} are the thermal expansion coefficients in the (n, s, z) coordinate system. The components (α_z, α_{sz}) are derived from the thermal expansion coefficients of the studied fibre materials (α_1, α_2) as follows

$$\alpha_z = \alpha_1 \cos^2\theta + \alpha_2 \sin^2\theta, \tag{15a}$$

$$\alpha_{sz} = \left(\alpha_1 - \alpha_2\right) \sin\theta \cos\theta. \tag{15b}$$

2.5. Hybrid series solution

Based on the Ritz method, the displacement field can be approximated as follows

$$\left\{U_x, U_y, \phi\right\}(z) = \sum_{j=1}^{m} \phi_j(z) \left\{U_{xj}, U_{yj}, \phi_j\right\}, \tag{16a}$$

$$\left\{U_z, \varsigma_y, \varsigma_x, \varsigma_\omega\right\}(z) = \sum_{j=1}^{m} \phi'_j(z) \left\{U_{zj}, \varsigma_{yj}, \varsigma_{xj}, \varsigma_{\omega j}\right\}, \tag{16b}$$

where $U_{xj}, U_{yj}, \phi_j, U_{zj}, \varsigma_{yj}, \varsigma_{xj}, \varsigma_{\omega j}$ are the unknowns to be computed; $\phi_j(z)$ is the shape functions which satisfy the boundary conditions (BCs) (Table 1).

Table 1. Shape functions and essential BCs of laminated composite thin-walled I-beams

BC	$\phi_j(x)/e^{\frac{-jx}{L}}$	$x=0$	$x=L$
S-S	$\sin\left(\frac{\pi x}{L}\right)$	$U_x=U_y=\phi=0$	$U=V=\phi=0$
C-F	$\sin^2\left(\frac{\pi x}{2L}\right)$	$U_x=U_y=\phi=0$ $U'_x=U'_y=\phi'=0$ $U_z=\varsigma_y=\varsigma_x=\varsigma_\omega=0$	
C-C	$\sin^2\left(\frac{\pi x}{L}\right)$	$U_x=U_y=\phi=0$ $U'_x=U'_y=\phi'=0$ $U_z=\varsigma_y=\varsigma_x=\varsigma_\omega=0$	$U_x=U_y=\phi=0$ $U'_x=U'_y=\phi'=0$ $U_z=\varsigma_y=\varsigma_x=\varsigma_\omega=0$

Substituting Eq. (16) in to Eqs. (10) and (11), and then applying Hamilton's principle lead to the characteristic equation for the buckling analysis of the laminated composite thin-walled beams as follows

$$\mathbf{K}\mathbf{p}=\mathbf{0}, \tag{17}$$

where $\mathbf{p}=\begin{bmatrix}\mathbf{U}_z & \mathbf{U}_x & \mathbf{U}_y & \boldsymbol{\Phi} & \varsigma_x & \varsigma_y & \varsigma_\omega\end{bmatrix}^T$ is the displacement vector; $\mathbf{K}$ is the stiffness matrix and is given as

$$\mathbf{K}=\begin{bmatrix}
\mathbf{K}^{11} & \mathbf{K}^{12} & \mathbf{K}^{13} & \mathbf{K}^{14} & \mathbf{K}^{15} & \mathbf{K}^{16} & \mathbf{K}^{17}\\
{}^T\mathbf{K}^{12} & \mathbf{K}^{22} & \mathbf{K}^{23} & \mathbf{K}^{24} & \mathbf{K}^{25} & \mathbf{K}^{26} & \mathbf{K}^{27}\\
{}^T\mathbf{K}^{13} & {}^T\mathbf{K}^{23} & \mathbf{K}^{33} & \mathbf{K}^{34} & \mathbf{K}^{35} & \mathbf{K}^{36} & \mathbf{K}^{37}\\
{}^T\mathbf{K}^{14} & {}^T\mathbf{K}^{24} & {}^T\mathbf{K}^{34} & \mathbf{K}^{44} & \mathbf{K}^{45} & \mathbf{K}^{46} & \mathbf{K}^{47}\\
{}^T\mathbf{K}^{15} & {}^T\mathbf{K}^{25} & {}^T\mathbf{K}^{35} & {}^T\mathbf{K}^{45} & \mathbf{K}^{55} & \mathbf{K}^{56} & \mathbf{K}^{57}\\
{}^T\mathbf{K}^{16} & {}^T\mathbf{K}^{26} & {}^T\mathbf{K}^{36} & {}^T\mathbf{K}^{46} & {}^T\mathbf{K}^{56} & \mathbf{K}^{66} & \mathbf{K}^{67}\\
{}^T\mathbf{K}^{17} & {}^T\mathbf{K}^{27} & {}^T\mathbf{K}^{37} & {}^T\mathbf{K}^{47} & {}^T\mathbf{K}^{57} & {}^T\mathbf{K}^{67} & \mathbf{K}^{77}
\end{bmatrix}, \tag{18}$$

with the following matrix elements

$$K_{ij}^{11}=E_{11}\int_0^L \phi_i''\phi_j''\mathrm{d}z,\quad K_{ij}^{12}=E_{16}\int_0^L \phi_i''\phi_j'\mathrm{d}z,\quad K_{ij}^{13}=E_{17}\int_0^L \phi_i''\phi_j'\mathrm{d}z,$$

$$K_{ij}^{14}=(E_{15}+E_{18})\int_0^L \phi_i''\phi_j'\mathrm{d}z,\quad K_{ij}^{15}=E_{12}\int_0^L \phi_i''\phi_j''\mathrm{d}z+E_{16}\int_0^L \phi_i'\phi_j\mathrm{d}z,$$

$$K_{ij}^{16}=E_{13}\int_0^L \phi_i''\phi_j''\mathrm{d}z+E_{17}\int_0^L \phi_i''\phi_j'\mathrm{d}z,\quad K_{ij}^{17}=E_{14}\int_0^L \phi_i''\phi_j''\mathrm{d}z+(E_{18}-E_{15})\int_0^L \phi_i''\phi_j'\mathrm{d}z,$$

$$K_{ij}^{22} = E_{66} \int_0^L \phi_i' \phi_j' \mathrm{d}z + \left(N_0^m + N_0^t\right) \int_0^L \phi_i' \phi_j' \mathrm{d}z, \quad K_{ij}^{23} = E_{67} \int_0^L \phi_i' \phi_j' \mathrm{d}z,$$

$$K_{ij}^{24} = (E_{56} + E_{68}) \int_0^L \phi_i' \phi_j' \mathrm{d}z + \left(N_0^m + N_0^t\right) y_p \int_0^L \phi_i' \phi_j' \mathrm{d}z,$$

$$K_{ij}^{25} = E_{26} \int_0^L \phi_i' \phi_j'' \mathrm{d}z + E_{66} \int_0^L \phi_i' \phi_j' \mathrm{d}z, \quad K_{ij}^{26} = E_{36} \int_0^L \phi_i' \phi_j' \mathrm{d}z + E_{67} \int_0^L \phi_i' \phi_j' \mathrm{d}z,$$

$$K_{ij}^{27} = E_{46} \int_0^L \phi_i' \phi_j'' \mathrm{d}z + (E_{68} - E_{56}) \int_0^L \phi_i' \phi_j' \mathrm{d}z, \quad K_{ij}^{33} = E_{77} \int_0^L \phi_i' \phi_j' \mathrm{d}z + \left(N_0^m + N_0^t\right) \int_0^L \phi_i' \phi_j' \mathrm{d}z,$$

$$K_{ij}^{34} = (E_{57} + E_{78}) \int_0^L \phi_i' \phi_j' \mathrm{d}z - \left(N_0^m + N_0^t\right) x_p \int_0^L \phi_i' \phi_j' \mathrm{d}z, \quad K_{ij}^{35} = E_{27} \int_0^L \phi_i' \phi_j'' \mathrm{d}z + E_{67} \int_0^L \phi_i' \phi_j' \mathrm{d}z,$$

$$K_{ij}^{36} = E_{37} \int_0^L \phi_i' \phi_j'' \mathrm{d}z + E_{77} \int_0^L \phi_i' \phi_j' \mathrm{d}z, \quad K_{ij}^{37} = E_{47} \int_0^L \phi_i' \phi_j'' \mathrm{d}z + (E_{78} - E_{57}) \int_0^L \phi_i' \phi_j' \mathrm{d}z,$$

$$K_{ij}^{44} = (E_{55} + 2E_{58} + E_{88}) \int_0^L \phi_i' \phi_j' \mathrm{d}z + \frac{\left(N_0^m + N_0^t\right) I_p}{A} \int_0^L \phi_i' \phi_j' \mathrm{d}z,$$

$$K_{ij}^{45} = (E_{25} + E_{28}) \int_0^L \phi_i' \phi_j'' \mathrm{d}z + (E_{56} + E_{68}) \int_0^L \phi_i' \phi_j' \mathrm{d}z,$$

$$K_{ij}^{46} = (E_{35} + E_{38}) \int_0^L \phi_i' \phi_j'' \mathrm{d}z + (E_{57} + E_{78}) \int_0^L \phi_i' \phi_j' \mathrm{d}z,$$

$$K_{ij}^{47} = (E_{45} + E_{48}) \int_0^L \phi_i' \phi_j'' \mathrm{d}z + (E_{88} - E_{55}) \int_0^L \phi_i' \phi_j' \mathrm{d}z,$$

$$K_{ij}^{55} = E_{22} \int_0^L \phi_i'' \phi_j'' \mathrm{d}z + E_{26} \int_0^L \left(\phi_i'' \phi_j' + \phi_i' \phi_j''\right) \mathrm{d}z + E_{66} \int_0^L \phi_i' \phi_j' \mathrm{d}z,$$

$$K_{ij}^{56} = E_{23} \int_0^L \phi_i'' \phi_j'' \mathrm{d}z + E_{27} \int_0^L \phi_i'' \phi_j' \mathrm{d}z + E_{36} \int_0^L \phi_i' \phi_j'' \mathrm{d}z + E_{67} \int_0^L \phi_i' \phi_j' \mathrm{d}z,$$

$$K_{ij}^{57} = E_{24} \int_0^L \phi_i'' \phi_j'' \mathrm{d}z + (E_{28} - E_{25}) \int_0^L \phi_i'' \phi_j' \mathrm{d}z + E_{46} \int_0^L \phi_i' \phi_j'' \mathrm{d}z + (E_{68} - E_{56}) \int_0^L \phi_i' \phi_j' \mathrm{d}z,$$

$$
\begin{aligned}
K_{ij}^{66} &= E_{33}\int_0^L \phi_i''\phi_j''\mathrm{d}z + E_{37}\int_0^L \left(\phi_i''\phi_j' + \phi_i'\phi_j''\right)\mathrm{d}z + E_{77}\int_0^L \phi_i'\phi_j'\mathrm{d}z,\\
K_{ij}^{67} &= E_{34}\int_0^L \phi_i''\phi_j''\mathrm{d}z + (E_{38}-E_{35})\int_0^L \phi_i''\phi_j'\mathrm{d}z + E_{47}\int_0^L \phi_i'\phi_j''\mathrm{d}z + (E_{78}-E_{57})\int_0^L \phi_i'\phi_j'\mathrm{d}z,\\
K_{ij}^{77} &= E_{44}\int_0^L \phi_i''\phi_j''\mathrm{d}z + (E_{48}-E_{45})\int_0^L \left(\phi_i''\phi_j' + \phi_i'\phi_j''\right)\mathrm{d}z + (E_{88}-2E_{58}+E_{55})\int_0^L \phi_i'\phi_j'\mathrm{d}z.
\end{aligned}
\tag{19}
$$

The buckling responses of the laminated composite thin-walled beam can be obtained by solving $\det(\mathbf{K}) = \mathbf{0}$.

3. NUMERICAL RESULTS

The laminated composite thin-walled I-beam in this numerical study is made of glass-epoxy materials with the following properties: $E_1 = 53.78$ GPa, $E_2 = 17.93$ GPa, $G_{12} = G_{13} = 8.96$ GPa, $G_{23} = 3.45$ GPa, $\nu_{12} = 0.25$. The thermal expansion coefficients of glass and epoxy are $\alpha_1 = 6.7\times10^{-7}\,\mathrm{K}^{-1}$ and $\alpha_2 = 3.6\times10^{-6}\,\mathrm{K}^{-1}$ respectively. The geometry of the laminated composite thin-walled I-beam is shown in Fig. 2 with $b_1 = b_2 = b_3 = 0.05$ m, $h_1 = h_2 = h_3 = 0.00208$ m.

3.1. Convergence and verification study

This section conducts convergence study of the present solution for buckling analysis of laminated composite thin-walled I-beams under mechanical loads. For Table 2, the laminated composite I-beam's length is expressed as $L/b_3 = 40$. The laminated angle-ply for all the flanges and web is $[45^\circ/-45^\circ]_{4s}$. It can be observed in Table 2 that the results of this paper's approach achieve numerical convergence at $m = 8$ and agree with the results of Nguyen et al. [34]. Therefore, the series number $m = 8$ is applied in subsequent analyses.

To further verify the current solution in mechanical environment, Table 3 presents the effects of the various fibre angle lay-ups, boundary conditions and the length-to-depth ratio on the laminated composite I-beam's critical buckling loads. It can be seen that in both cases of $L/b_3 = 20$ and $L/b_3 = 80$, the critical buckling loads decrease with the increasing fibre angle θ° of the $[\theta^\circ, -\theta^\circ]_{4s}$ lay-up. The buckling results of the laminated composite I-beam with S-S boundary condition and $L/b_3 = 80$, C-F boundary condition and $L/b_3 = 20$ show good agreements with past researches from Kim et al. [35] and Vo and Lee [18]. More results are computed for the laminated composite I-beam set-up in Table 3 but with more cases of fibre angle θ°. These results are plotted for $L/b_3 = 20$ and $L/b_3 = 80$ in Fig. 3.

Table 2. Convergence of critical buckling loads (kN) for the laminated composite thin-walled I-beams under mechanical load

BCs	Reference	m					
		2	4	6	8	10	12
S-S	Present	2.931	2.679	2.671	2.671	2.671	2.671
	Nguyen et al. (Shear) [34]	2.752	2.690	2.671	2.671	2.671	2.671
	Nguyen et al. (No shear) [34]	2.755	2.692	2.673	2.673	2.673	2.673
C-F	Present	3.852	1.564	0.738	0.671	0.668	0.669
	Nguyen et al. (Shear) [34]	0.706	0.668	0.668	0.668	0.668	0.668
	Nguyen et al. (No shear) [34]	0.706	0.668	0.668	0.668	0.668	0.668
C-C	Present	10.768	10.659	10.657	10.657	10.657	10.657
	Nguyen et al. (Shear) [34]	10.797	10.678	10.657	10.657	10.657	10.657
	Nguyen et al. (No shear) [34]	10.832	10.712	10.691	10.691	10.691	10.691

Table 3. Comparison of critical buckling loads (N) of the thin-walled composite I-beams under mechanical loads

BC	Reference	Fibre angle							
		$[0]_{16}$	$[15/\text{-}15]_{4s}$	$[30/\text{-}30]_{4s}$	$[45/\text{-}45]_{4s}$	$[60/\text{-}60]_{4s}$	$[75/\text{-}75]_{4s}$	$[90/\text{-}90]_{4s}$	$[0/90]_{4s}$
$L/b_3 = 80$									
S-S	Present (Shear)	1438.1	1299.4	965.0	668.1	528.6	487.0	479.6	959.0
	Kim et al. (No shear) [35]	1438.8	1300.0	965.2	668.2	528.7	487.1	-	959.3
C-F	Present (Shear)	361.2	326.4	242.4	167.8	132.7	122.3	120.4	240.9
C-C	Present (Shear)	5743.3	5191.0	3856.8	2670.6	2113.2	1946.7	1917.1	3831.4
$L/b_3 = 20$									
S-S	Present (Shear)	22832.7	20660.1	15376.7	10657.3	8433.9	7767.7	7648.6	15255.8
C-F	Present (Shear)	5768.6	5213.8	3873.7	2682.4	2122.5	1955.2	1925.5	3848.3
	Vo and Lee (Shear) [18]	5741.5	5189.0	3854.5	2668.4	2111.3	1945.1	-	3829.8
	Kim et al. (No shear) [35]	5755.2	5199.8	3861.0	2672.7	2114.7	1948.3	-	3857.8
C-C	Present (Shear)	77772.9	72116.0	57102.8	42069.5	33438.5	30632.4	29873.4	53993.2

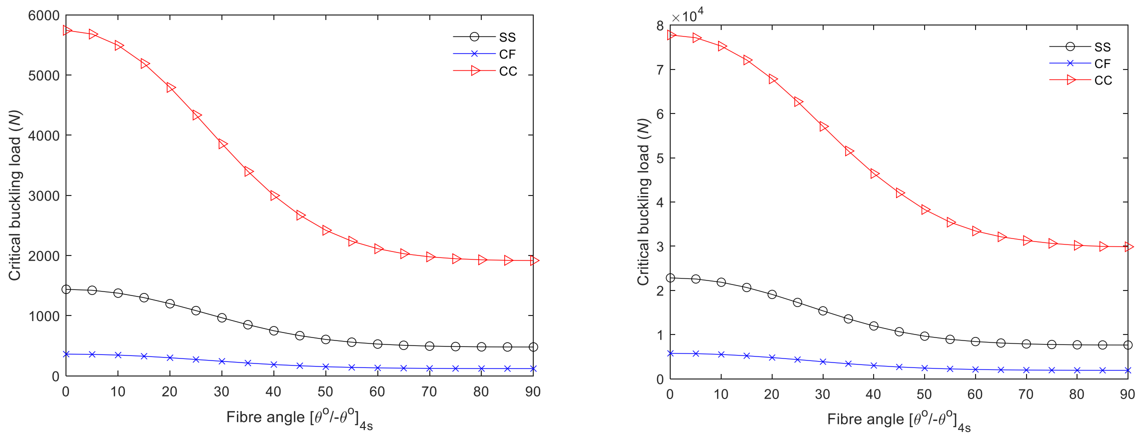

(a) $L/b_3 = 80$ (b) $L/b_3 = 20$

Fig. 3. Critical buckling loads (N) for the glass-epoxy composite I-beam with respect to fibre angle for different boundary conditions

3.2. Thermal buckling stability

This section aims to study the effect of fibre angle, length-to-depth ratio and boundary conditions on the thermal buckling stability of the laminated composite thin-walled I-beams. The critical buckling temperature for various fibre angle lay-ups, boundary conditions and length-to-depth ratios are plotted in Fig. 4. It can be seen that the critical buckling temperature slightly increases when θ° goes from 0° to 20° and drop sharply

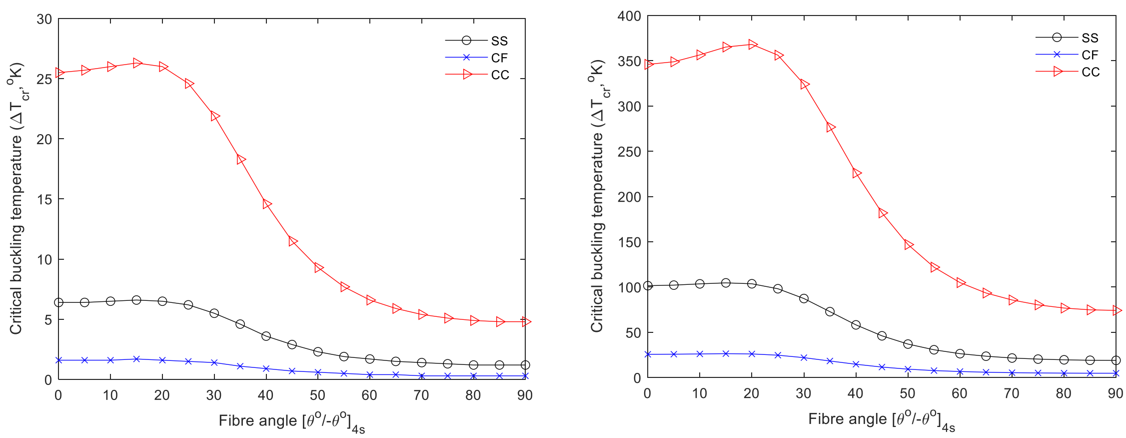

(a) $L/b_3 = 80$ (b) $L/b_3 = 20$

Fig. 4. Critical buckling temperature ΔT_{cr} ($^\circ$K) for the glass-epoxy composite I-beam

when θ° is in the range of 20°–70° before plateauing afterwards. This trend is particularly clearer when the beam is under C-C boundary condition.

Moreover, the laminated composite I-beam can withstand much more temperature rise and thermal load with $L/b_3 = 20$ compared to $L/b_3 = 80$. Fig.5 demonstrates better the effects of length-to-depth ratios on the thermal buckling stability of the laminated composite I-beams. The thin-walled beam is drastically more stable at low L/b_3 and the L/b_3 becomes less significant when $L/b_3 > 30$.

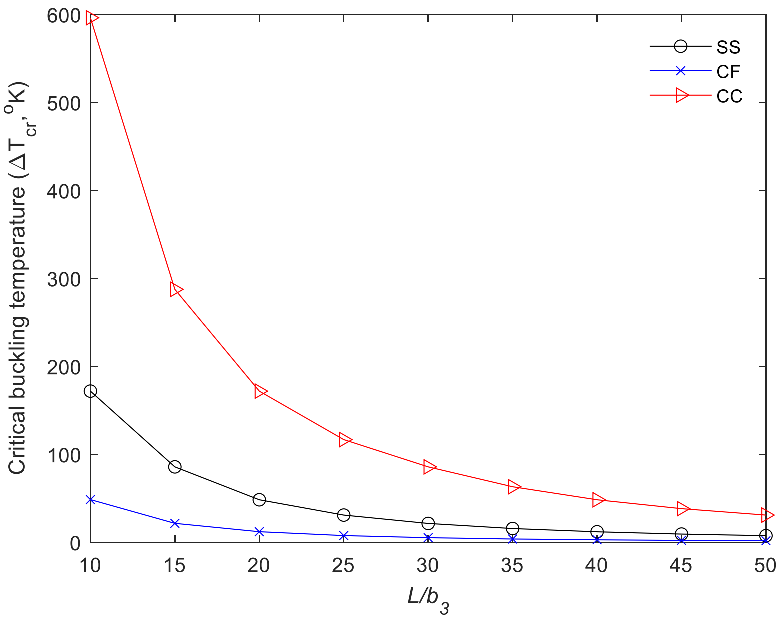

Fig. 5. Critical buckling temperature ΔT_{cr} (°K) for the laminated composite I-beam with various length-to-depth ratios ($[0^\circ/90^\circ]_{4s}$)

4. CONCLUSION

A shear-deformable thin-walled beam model and a hybrid series solution are presented in this study. The glass-epoxy composite I-beam is investigated for its mechanical and thermal buckling stability. This model can predict accurately the critical buckling loads and critical buckling temperature for different beam configurations. The effects of fibre angle lay-up, boundary conditions and length-to-depth ratios are shown in the numerical results. The beam's buckling capacity is higher for low fibre angle, low length-to-depth ratios and clamped-clamped boundary condition. The present model is shown to be valid for buckling analysis of laminated composite I-beam under mechanical and thermal loads.

DECLARATION OF COMPETING INTEREST

The authors declare that they have no known competing financial interests or personal relationships that could have appeared to influence the work reported in this paper.

FUNDING

This research received no specific grant from any funding agency in the public, commercial, or not-for-profit sectors.

REFERENCES

[1] O. A. Bauchau and J. I. Craig. *Structural analysis: with applications to aerospace structures*. Springer Netherlands, (2009).

[2] T. H. G. Megson. *Aircraft structures for engineering students*. United Kingdom: Butterworth-Heinemann, seventh edition, (2021).

[3] S. Eken. Free vibration analysis of composite aircraft wings modeled as thin-walled beams with NACA airfoil sections. *Thin-Walled Structures*, **139**, (2019), pp. 362–371. https://doi.org/10.1016/j.tws.2019.01.042.

[4] Z. K. Awad, T. Aravinthan, Y. Zhuge, and F. Gonzalez. A review of optimization techniques used in the design of fibre composite structures for civil engineering applications. *Materials & Design*, **33**, (2012), pp. 534–544. https://doi.org/10.1016/j.matdes.2011.04.061.

[5] C. Mittelstedt. Buckling and post-buckling of thin-walled composite laminated beams—a review of engineering analysis methods. *Applied Mechanics Reviews*, **72**, (2020). https://doi.org/10.1115/1.4045680.

[6] L. Librescu and O. Song. *Thin-walled composite beams*. Springer Netherlands, (2006). https://doi.org/10.1007/1-4020-4203-5.

[7] N. R. Bauld and T. Lih-Shyng. A Vlasov theory for fiber-reinforced beams with thin-walled open cross sections. *International Journal of Solids and Structures*, **20**, (3), (1984), pp. 277–297. https://doi.org/10.1016/0020-7683(84)90039-8.

[8] M. D. Pandey, M. Z. Kabir, and A. N. Sherbourne. Flexural-torsional stability of thin-walled composite I-section beams. *Composites Engineering*, **5**, (1995), pp. 321–342. https://doi.org/10.1016/0961-9526(94)00101-e.

[9] J. Lee and S.-E. Kim. Free vibration of thin-walled composite beams with I-shaped cross-sections. *Composite Structures*, **55**, (2002), pp. 205–215. https://doi.org/10.1016/s0263-8223(01)00150-7.

[10] J. Lee and S.-E. Kim. Flexural–torsional buckling of thin-walled I-section composites. *Computers & Structures*, **79**, (2001), pp. 987–995. https://doi.org/10.1016/s0045-7949(00)00195-4.

[11] A. G. Razaqpur and H. Li. Thin-walled multicell box-girder finite element. *Journal of Structural Engineering*, **117**, (1991), pp. 2953–2971. https://doi.org/10.1061/(asce)0733-9445(1991)117:10(2953).

[12] R. Pavazza, A. Matoković, and M. Vukasović. A theory of torsion of thin-walled beams of arbitrary open sections with influence of shear. *Mechanics Based Design of Structures and Machines*, **50**, (2020), pp. 206–241. https://doi.org/10.1080/15397734.2020.1714449.

[13] S. Y. Back and K. M. Will. Shear-flexible thin-walled element for composite I-beams. *Engineering Structures*, **30**, (2008), pp. 1447–1458. https://doi.org/10.1016/j.engstruct.2007.08.002.

[14] S. S. Maddur and S. K. Chaturvedi. Laminated composite open profile sections: non-uniform torsion of I-sections. *Composite Structures*, **50**, (2000), pp. 159–169. https://doi.org/10.1016/s0263-8223(00)00093-3.

[15] S. S. Maddur and S. K. Chaturvedi. Laminated composite open profile sections: first order shear deformation theory. *Composite Structures*, **45**, (1999), pp. 105–114. https://doi.org/10.1016/s0263-8223(99)00005-7.

[16] J. Lee. Flexural analysis of thin-walled composite beams using shear-deformable beam theory. *Composite Structures*, **70**, (2005), pp. 212–222. https://doi.org/10.1016/j.compstruct.2004.08.023.

[17] Z. Qin and L. Librescu. On a shear-deformable theory of anisotropic thin-walled beams: further contribution and validations. *Composite Structures*, **56**, (2002), pp. 345–358. https://doi.org/10.1016/s0263-8223(02)00019-3.

[18] T. P. Vo and J. Lee. Flexural–torsional coupled vibration and buckling of thin-walled open section composite beams using shear-deformable beam theory. *International Journal of Mechanical Sciences*, **51**, (2009), pp. 631–641. https://doi.org/10.1016/j.ijmecsci.2009.05.001.

[19] J. Lee. Center of gravity and shear center of thin-walled open-section composite beams. *Composite Structures*, **52**, (2001), pp. 255–260. https://doi.org/10.1016/s0263-8223(00)00177-x.

[20] S. N. Jung and J.-Y. Lee. Closed-form analysis of thin-walled composite I-beams considering non-classical effects. *Composite Structures*, **60**, (2003), pp. 9–17. https://doi.org/10.1016/s0263-8223(02)00318-5.

[21] N.-I. Kim and D. K. Shin. Coupled deflection analysis of thin-walled Timoshenko laminated composite beams. *Computational Mechanics*, **43**, (2008), pp. 493–514. https://doi.org/10.1007/s00466-008-0324-9.

[22] L. Wu and M. Mohareb. Finite element formulation for shear deformable thin-walled beams. *Canadian Journal of Civil Engineering*, **38**, (2011), pp. 383–392. https://doi.org/10.1139/l11-007.

[23] A. Prokić. On fivefold coupled vibrations of Timoshenko thin-walled beams. *Engineering Structures*, **28**, (2006), pp. 54–62. https://doi.org/10.1016/j.engstruct.2005.07.002.

[24] S. J. Kim, K. W. Yoon, and S. N. Jung. Shear correction factors for thin-walled composite boxbeam considering nonclassical behaviors. *Journal of Composite Materials*, **30**, (1996), pp. 1132–1149. https://doi.org/10.1177/002199839603001004.

[25] X.-B. Bui, T.-K. Nguyen, N.-D. Nguyen, and T. P. Vo. A general higher-order shear deformation theory for buckling and free vibration analysis of laminated thin-walled composite I-beams. *Composite Structures*, **295**, (2022). https://doi.org/10.1016/j.compstruct.2022.115775.

[26] R. F. Vieira, F. B. E. Virtuoso, and E. B. R. Pereira. A higher order thin-walled beam model including warping and shear modes. *International Journal of Mechanical Sciences*, **66**, (2013), pp. 67–82. https://doi.org/10.1016/j.ijmecsci.2012.10.009.

[27] N.-L. Nguyen, G.-W. Jang, S. Choi, J. Kim, and Y. Y. Kim. Analysis of thin-walled beam-shell structures for concept modeling based on higher-order beam theory. *Computers & Structures*, **195**, (2018), pp. 16–33. https://doi.org/10.1016/j.compstruc.2017.09.009.

[28] L. C. Trinh, T. P. Vo, H.-T. Thai, and T.-K. Nguyen. An analytical method for the vibration and buckling of functionally graded beams under mechanical and thermal loads. *Composites Part B: Engineering*, **100**, (2016), pp. 152–163. https://doi.org/10.1016/j.compositesb.2016.06.067.

[29] T.-K. Nguyen, B.-D. Nguyen, T. P. Vo, and H.-T. Thai. Hygro-thermal effects on vibration and thermal buckling behaviours of functionally graded beams. *Composite Structures*, **176**, (2017), pp. 1050–1060. https://doi.org/10.1016/j.compstruct.2017.06.036.

[30] X. Li, Y. H. Li, and Y. Qin. Free vibration characteristics of a spinning composite thin-walled beam under hygrothermal environment. *International Journal of Mechanical Sciences*, **119**, (2016), pp. 253–265. https://doi.org/10.1016/j.ijmecsci.2016.10.028.

[31] Y. Sun, S.-R. Li, and R. C. Batra. Thermal buckling and post-buckling of FGM Timoshenko beams on nonlinear elastic foundation. *Journal of Thermal Stresses*, **39**, (2016), pp. 11–26. https://doi.org/10.1080/01495739.2015.1120627.

[32] S. K. Simonetti, G. Turkalj, and D. Lanc. Thermal buckling analysis of thin-walled closed section FG beam-type structures. *Thin-Walled Structures*, **181**, (2022). https://doi.org/10.1016/j.tws.2022.110075.

[33] D. Pantousa. Numerical study on thermal buckling of empty thin-walled steel tanks under multiple pool-fire scenarios. *Thin-Walled Structures*, **131**, (2018), pp. 577–594. https://doi.org/10.1016/j.tws.2018.07.025.

[34] N.-D. Nguyen, T.-K. Nguyen, T. P. Vo, T.-N. Nguyen, and S. Lee. Vibration and buckling behaviours of thin-walled composite and functionally graded sandwich I-beams. *Composites Part B: Engineering*, **166**, (2019), pp. 414–427. https://doi.org/10.1016/j.compositesb.2019.02.033.

[35] N.-I. Kim, D. K. Shin, and M.-Y. Kim. Flexural–torsional buckling loads for spatially coupled stability analysis of thin-walled composite columns. *Advances in Engineering Software*, **39**, (2008), pp. 949–961. https://doi.org/10.1016/j.advengsoft.2008.03.001.